Self-assembled DNA–cationic-lipid complexes: Two-dimensional smectic ordering, correlations, and interactions

T. Salditt,* I. Koltover, J. O. Rädler,† and C. R. Safinya
Materials Department, Physics Department, and Biochemistry and Molecular Biology Program, University of California, Santa Barbara, California 93106
(Received 12 February 1998)

We report a synchrotron small-angle x-ray scattering (SAXS) study of the mutilayered, self-assembled structure (complex) that is formed by mixing DNA with cationic liposomes. In these complexes the DNA is confined between charged lipid bilayers and orders as a two-dimensional (2D) smectic liquid crystal. The power-law bilayer-bilayer correlations of the 3D multilayer smectic liquid crystal, which are coupled to the 2D lattice of DNA chains, are found to deviate significantly from those described by the standard Caillé model of smectic-*A* phases. To model the DNA ordering, the 2D smectic correlation function and the corresponding structure factor are derived from the smectic Hamiltonian in harmonic approximation. The resulting line shape is then fitted to the DNA correlation peak. It is found that for samples of higher d, short-range correlations between the DNA in adjacent sheets have to be assumed to explain the data. From the least-square fitting, the 2D DNA interchain compressibility modulus B is extracted as a function of d and discussed in view of different possible microscopic interactions responsible for the ordering. [S1063-651X(98)10207-6]

PACS number(s): 87.22.Bt, 61.10.Eq, 61.30.Eb

I. INTRODUCTION

Recently, a novel multilamellar structure of DNA sandwiched in between cationic lipid membranes has been reported by Rädler *et al.* [1,2]. The structure is formed in a self-assembled manner when mixing suspensions of cationic lipid vesicles (cationic liposomes) with DNA. Such complexes have been shown to be able to mimic certain characteristics of natural viruses in their ability to act as efficient chemical carriers of extracellular DNA across outer cell membranes and nuclear membranes (transfection) for gene therapy applications [3]. The correlation of the gene carrier mechanism and transfection efficiency to the microscopic structure of the complex remains a fascinating challenge for the near future. At the same time, the statistical physics of the complexes exhibit interesting ordering and fluctuation phenomena, which are currently studied in several theoretical works [4–6]. More generally, the self-assembly of supramolecular structures, and in particular the interaction of membranes and polymers, is currently an active area of research [7,8].

In the case of the structurally well defined DNA macromolecule, the ability to produce perfectly monodispersed DNA has led to many important experimental studies in solution over the past two decades [9]. These include studies as a model system for direct observation of chain reptation dynamics [10], and persistence-length measurements in polyelectrolytes [11]. Structural studies have been designed to elucidate the various mechanisms by which giant DNA molecules are able to undergo dense conformations, with possible similarity to their biologically active native state, either induced by multivalent cations [12], or in high density liquid crystalline phases, both *in vitro* and *in vivo* in packing of DNA in bacteria and eukaryotic cells [13]. Theoretically, a high density phase of DNA chains has been predicted with a novel ''braided chiral'' structure with crystalline order [14]. With the obvious relevance of DNA and given the present understanding of the macromolecule in solution, the elucidation of its interaction with other macromolecular assemblies is of fundamental interest.

In this work we report a quantitative synchrotron x-ray scattering study elucidating the nature of the DNA ordering in two-dimensional (2D) layers confined between the lipid bilayers of the complexes. A 2D smectic order is inferred from the analysis of the line shape of the DNA correlation peak for samples of different average spacing d between DNA. Furthermore, for larger d we find additional *cross*-correlations between the DNA of adjacent layers. The elastic constants extracted from the least-square fitting of the correlation peak indicate a repulsive long-ranged electrostatic interaction.

The structure and positional correlations of low dimensional systems are often governed by strong thermal fluctuations. In the case of smectic symmetry, for example, the lower critical dimension is three (3D). In 3D, true long range order breaks down and is replaced by an algebraic decay of correlations. This Landau-Peierls instability has been investigated in detail both theoretically [15] and experimentally [16,17]. However, only few experimental studies have been reported on smectic phases below their lower critical dimension [18]. In this case, the positional correlations are weaker than algebraic, resulting in an anisotropic short range order. Related to the correlation functions are the interesting elastic properties of smectic phases, which have recently been studied in the framework of a nonlinear theory, in which the spacial fluctuations of smectic liquid crystals were related to

*Present address: Sektion Physik der Ludwig-Maximilians-Universität München, Geschwister-Scholl-Platz 1, 80539 München, Germany.
†Present address: Physikdepartment, TU München, 85747 Garching, Germany.

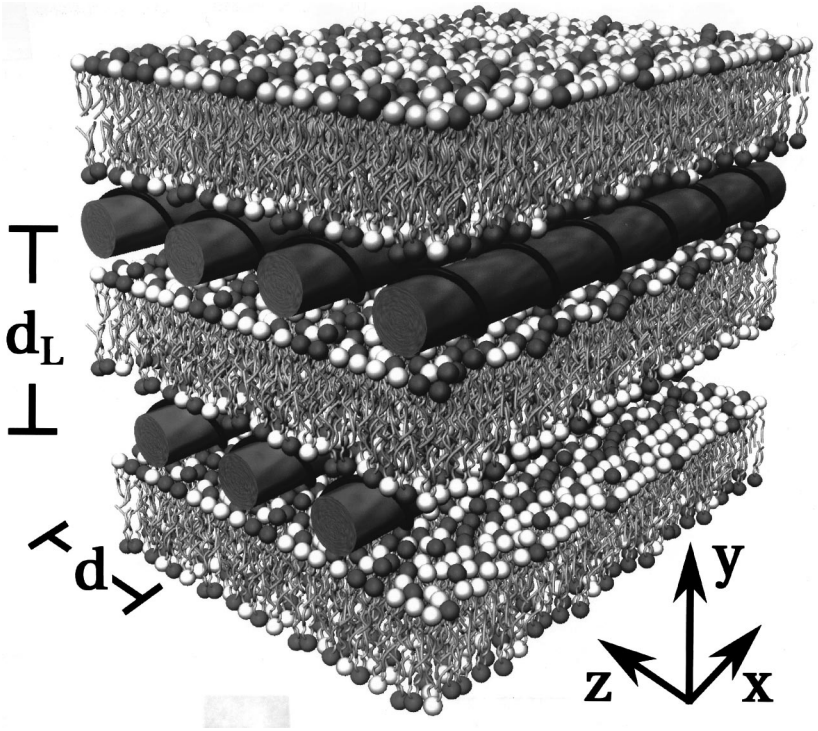

FIG. 1. Sketch of the self-assembled DNA-cationic liposome complex with the DNA double helices represented by rods in between the lipid membrane comprising the neutral and cationic lipids. The corresponding lipid headgroups are shown in light and dark shade, respectively. δ_m denotes the multilamellar periodicity and d the interhelical distance.

the spatiotemporal fluctuations of growing interfaces, in particular to the Kardar-Parisi-Zhang (KPZ) equation [19]. The elastic coefficients that contain much of the microscopic interactions governing a particular system can be determined from scattering experiments [16,17]. As a consequence of the Landau-Peierls effect, this becomes experimentally feasible in spite of often low cross sections, since the correlation peaks themselves refect the thermal scattering, unlike the thermal diffuse scattering in 3D crystals, which forms only a background to the Bragg peaks.

When mixing aqueous solutions of DNA with a suspension of cationic lipid vesicles (cationic liposomes), a highly condensed system (complex) is formed in a self-assembled manner, with the cationic lipids neutralized by the negative phosphate groups of the DNA. The driving force of the complex self-assembly is the entropic gain in releasing the counterions both from the cationic lipids and in particular from the DNA (Manning condensation) [20]. Multilamellar complex structures were observed for three types of DNA (λ phage, *Escherichia coli*, and pBR322 plasmid), and two different phospholipid systems consisting each of cationic DOTAP (dioleoyl-trimethylammonium-propane) and of DOPE (dioleoyl-phosphatidyl-ethanolamine) or DOPC (dioleoyl-phosphatidylcholine), respectively, [1]. In addition, complexes made out of λ-DNA and DLPC/DDAB (dilaureoyl-phosphatidylcholine/didodecyl-dimethyl-ammonium bromide), a lipid system with shorter hydrocarbon tails and therefore also smaller bilayer thickness δ_m, have been found to exhibit the same structure [21]. Thus the multilamellar phase is not specific to a certain DNA/lipid system, but of more general nature. In this work we will not repeat the complete line of arguments including experimental evidence from x-ray scattering as well as light microscopy experiments (double fluoresence, crossed polarizers, differential imaging contrast) [1], which led to the postulation of the multilamellar structure depicted in the schematic of Fig. 1. We will rather start from this structure as the basis and study the details of the DNA ordering from the line shape of the DNA correlation peak. The results will allow us to draw conclusions on the nature of the relevant microscopic interactions.

The paper is organized as follows. Section II gives a brief account of sample preparation and the setup of the SAXS experiment. The data will be presented with a discussion of the main features in the scattering distribution. In Sec. III the x-ray structure factor of a 2D smectic liquid crystal is derived from the Hamiltonian. Both ''single crystal'' and ''powder-averaged'' expressions are discussed. This part of the work is quite general and can be readily applied to the study of other 2D smectic systems. The model is then used to fit the DNA correlation peak for a series of samples. The results of the least-square fitting are presented in Sec. IV along with a discussion of the implications on the effective interactions between the DNA in the complex. Appendix A contains a detailed calculation of the 2D smectic correlation function, and Appendix B discusses the compressibility of a linear array of line charges.

II. MATERIALS AND METHODS

The samples were prepared by mixing λ phage DNA (48502 bp, contour length of 16.5 μm) with liposomes in ultrapure water, as described in [1]. The liposomes consisted of cationic DOTAP (dioleoyl-trimethylammonium-propane) and neutral DOPC (dioleoyl-phosphatidylcholine) at various weight ratios $\nu := \text{mass[DOPC]/mass[DOTAP]}$ (lipid dilutions), while keeping the the DOTAP/DNA weight ratio constant at 2.2 to ensure overall charge neutrality of the complexes. In this so-called isoelectric regime, the cationic groups of DOTAP exactly balance the negative base pairs of DNA. To assure a proper mixing of the two lipid types, they are matched in their respective chain length. By adjusting the

ratio of neutral to positive lipid component, the average interhelical spacing d between DNA can be controlled over a range of 27–60 Å, i.e., from an almost close-packed to a more diluted state. At higher dilution the system eventually phase separates to a phase of complexes in coexistence with a pure lipid lamellar phase [21].

Small-angle x-ray scattering (SAXS) experiments were performed with the samples sealed in the same quartz capillaries (1.5 mm diameter) in which they had been mixed. Consequently, the complexes were surrounded by excess water, corresponding to the volumes of the initial lipid and DNA stock solutions before the condensation of the complex phase. The resulting suspension of complexes was perfectly isotropic, as evidenced by powderlike Scherrer rings on an image plate detector. As observed with light microscopy, the complexes exhibit a globular structure with globule diameters on the order of 0.5 μm [1]. In the isoelectric regime (charge neutral complexes) the globules aggregate to larger clusters. Thus, on semimacroscopic length scales, the sample structure was not homogeneous. Indeed, x-ray scans taken at different positions of the capillary with respect to the beam typically showed large intensity variations. However, the curves overlapped perfectly after scaling the intensity, indicating an identical structure on the submicrometer scale.

SAXS measurements were carried out both at an in-house 18 kW rotating anode equipped with a bent graphite monochromator and a two-dimensional image plate detector, and at the Stanford Synchrotron Radiation Laboratory (SSRL). The high resolution data for line shape analysis were collected at the Wiggler beamlines 7-2 and 10-2 of SSRL, with the x-ray energy set to 8.047 keV and 10.00 keV, respectively, by double-bounce Si(111) monochromators. Higher harmonics were supressed by a mirror, which also focused the incoming beam in the horizontal plane with a convergence of 2 mrad yielding an out-of-plane resolution of $\simeq 0.008$ Å^{-1} (HWHM). In the (vertical) scattering plane the resolution was set by tight slits to 0.0013 Å^{-1} (HWHM) and 0.0006 Å^{-1} (HWHM), for the two instruments, respectively.

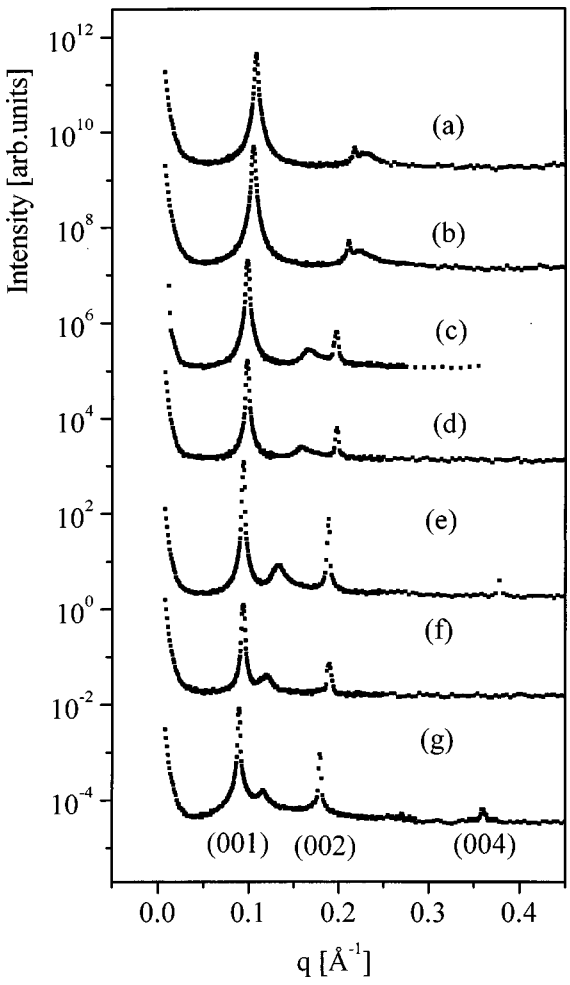

FIG. 2. Small-angle scattering of charge-neutral lipid/DNA complexes in excess water. Curves for samples of increasing ratios between neutral and cationic lipid ν are shifted by multiplicative factors: from top to bottom $\nu=0$, 0.35, 0.67, 1, 1.5, 2.33, and 3 [curves (a)–(g)]. Apart from very sharp Bragg reflections with the typical power-law tails of multilamellar phases, a much broader and weaker peak arising from DNA-DNA correlations is observed (vertical arrows).

III. SMALL-ANGLE X-RAY SCATTERING: LAMELLAR AND DNA DIFFRACTION PEAKS

SAXS scans for five representative samples in the isoelectric regime are displayed in Fig. 2 on a semilogarithmic scale, with the respective curves shifted by multiplicative constants for better comparison. Curves (a) through (g) correspond to $\nu=0$, 0.35, 0.67, 1, 1.5, 2.33, and 3. All samples show strong first- and second-order Bragg peaks (00l) of the lamellar structure. Some samples, in particular those of higher ν, additionally exhibit higher harmonics (004) and (005), while (003) is generally suppressed by a form factor minimum. Thus, the scattering distribution indicates a well ordered lamellar structure of stacked membranes, with a periodicity d_l that slightly increases from $d_l=57.8$ Å for $\nu=0$ up to $d_l=70.3$ Å for $\nu=3$. The width of the peaks is resolution limited, setting a lower bound of $L_m \simeq 2000$ Å for the domain lamellar domain sizes (the subscript m is carried on those variables that refer to the 3D smectic liquid crystal of the lipid membranes rather than the 2D smectic liquid crystal of the DNA). With an upper bound for L_m given by the diameter of the globules, one can conclude that the globules consist of only a few, or more likely, just one lamellar domain.

Apart from the lamellar peaks, the scans exhibit also a much broader and weaker maximum arising from the DNA-DNA correlations (vertical arrows), shifting over a wide range as a function of ν corresponding to a change in d spacing from an essentially closed packed structure of $d=26$ Å up to $d=54$ Å. This increase is governed by the relationship

$$d=\frac{A_D\rho_D}{\delta_m\rho_l}(L/D), \tag{1}$$

which results from simple mass conservation in the multilamellar geometry (neglecting the extra space that is left open due to defects of the DNA ordering), with A_D the DNA cross-sectional area, ρ_D and ρ_l the mass densities of DNA and lipid, respectively, δ_m the membrane thickness, and L/D the lipid to DNA mass ratio.

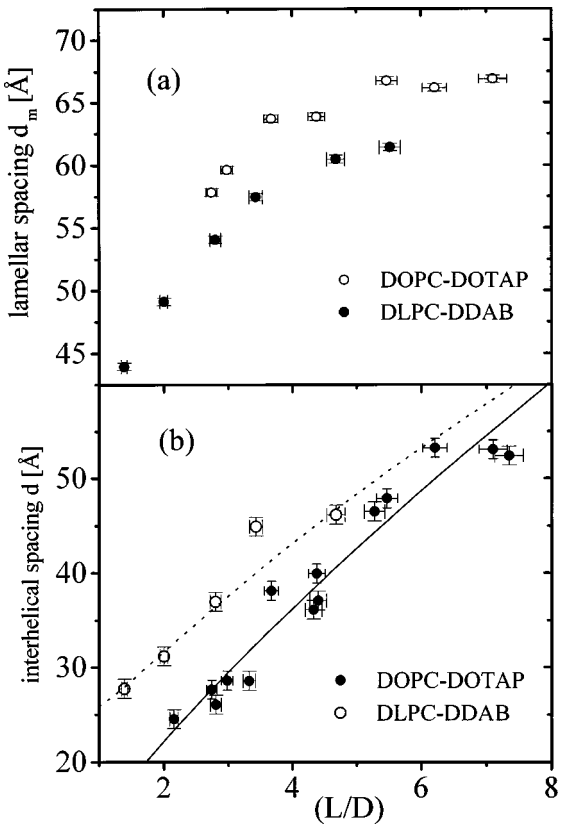

FIG. 3. The increase of (a) the multilamellar distance d_l and (b) the interhelical distance d with increasing total lipid to DNA ratio L/D (lipid dilution) for the system DOPC/DOTAP (solid circles) and DLPC/DDAB (open circles). The solid and dotted lines in (b) are the corresponding theoretic predictions according to Eq. (1).

Figure 3 shows the changes of the structural changes associated with the lipid dilution in the isoelectric regime. In Fig. 3(a) the variation of the multilamellar periodicities d_m is plotted versus the total lipid to DNA ratio L/D, for the DOPC/DOTAP (solid circles) and DLPC/DDAB systems (open circles). The systems differ mainly in the chain length leading to a much shorter δ_m and therefore also $d_m = \delta_w + \delta_m$ in the DLPC/DDAB case [22]. In each case the increase of d_m with L/D is due to the fact that the neutral colipid is always somewhat shorter than the cationic lipid. Therefore, δ_m of the combined systems intrapolates the two single-component values, which can be measured independently by water dilution in the pure lipid system without DNA. The average thickness of the water gap $\delta_w = d_m - \delta_m$ remains approximately constant corresponding to the diameter of DNA, $2r_D \simeq 20$ Å plus a hydration layer [1]. Figure 3(b) shows the DNA spacing d as a function of the lipid/DNA mass ratio for the two lipid systems, DOPC/DOTAP (solid circles) and DLPC/DDAB (open circles), with the corresponding dilution lines according to Eq. (1). The deviations from the linear behavior result from the changes in δ_m. These findings indicate that the lipid dilution law is generally valid for lamellar complex phases, as long as the neutral and cationic lipids do not phase separate [21].

Over the past decades a large body of experimental work has confirmed that fluctuations in multimamellar stacks of membranes or more generally lamellar phases of lipids or surfactants in solution are well described by the harmonic,

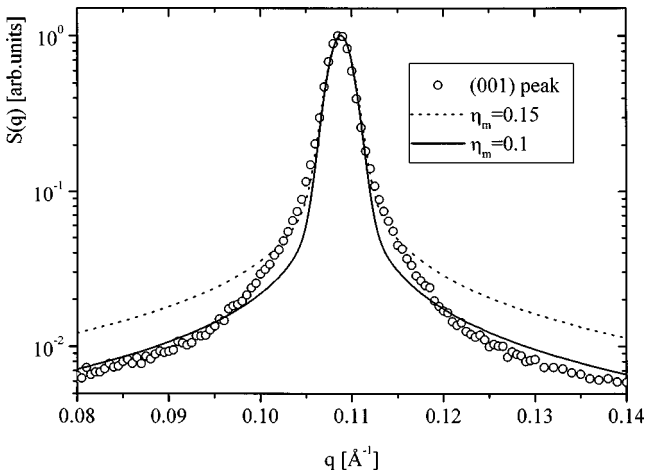

FIG. 4. The first lamellar peak (001) of the $\nu = 0$ sample. A pronounced deviation from Caillé's line shape is found; see the solid and dotted curves for parameters $\eta_m = 0.1$ and $\eta_m = 0.15$, respectively. In the simulations, the domain size was set to $L_m = 2000$ Å.

smectic Hamiltonian including terms of bending and compressional modes [16,17,23], resulting in the well-known Caillé line shape of the lamellar Bragg peaks [15]. A fundamental assumption in the derivation of that model is isotropy in the plane of the membrane. In the case of lipid/DNA complexes, however, the bending rigidity must locally be orientation dependent, with the rigidity enhanced in the direction along the stands. Given the high persistence length of about 500 Å, thermal height fluctuations along the y axis must therefore be totally suppressed at least on smaller length scales, while the system can support bending along x more easily. The compressional modes must also be affected by the DNA, reducing the fluctuations of the lamellar periodicity d_l due to electrostatic and hard core interaction, respectively. Moreover, from a more fundamental viewpoint, there must be additional terms in the Hamiltonian describing the modes of DNA and also the possible coupling between the fluctuations of the layers and those of DNA, see below.

In Fig. 4 the (001) peak of the $\nu = 0$ sample is shown on a semilogarithmic scale along with simulated line shapes of the Caillé type. Since the peak is symmetric, the line shape should only depend on the finite domain size L_m and the unitless parameter η_m containing a combination of the system's bending and compressional modulus. Clearly, the theoretical line shape does not explain the data. For higher values of η_m the central and medium $q - q_0$ range can be fitted, but not the tails. For lower values the tails can be fitted, but there are systematic deviations at small $q_- q_0$. This may suggest that, compared to the Caillé case, fluctuations on shorter wavelength are indeed suppressed. Figure 5 shows the left tails of the (001) peak after background subtraction on a double-logarithmic scale with an empirical power-law fit $I \propto q^{-\gamma}$ to the tail. The exponent γ extracted from the tails ranges between 1 and 2, while the Caillé model after powder averaging would give a value below 1, $\gamma \simeq 1 - \eta$ [17]. The systematic dependence of γ as a function of ν is depicted in the inset. For samples of decreasing DNA content, the deviation from the Caillé model gets less and less pronounced. One may argue that for very stiff lamellar systems with η_m

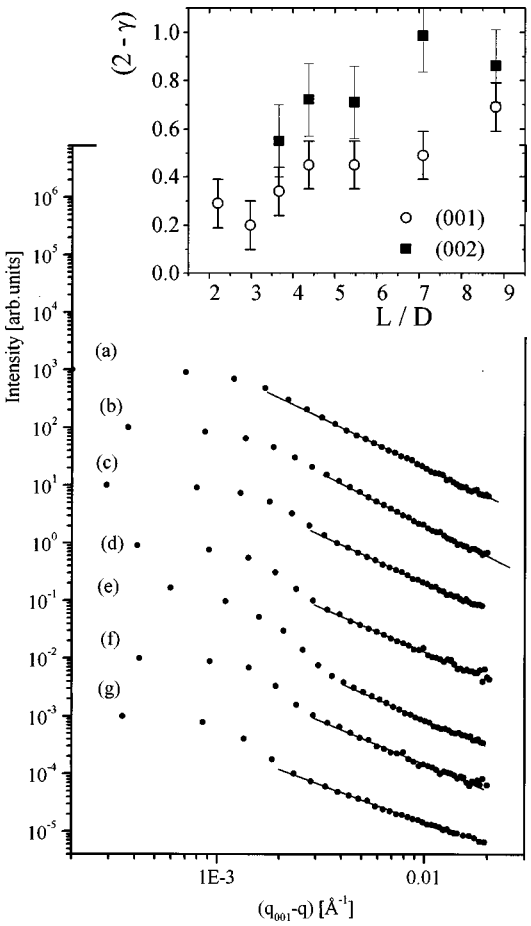

FIG. 5. The left tails of the (001) peaks on semilogarithmic scale after subtraction of a constant background level. The central width is resolution limited, and followed by a power-lay decay $S(q) \propto q^{-\gamma}$ over one decade in q. The results of the fits (solid lines) are plotted versus L/D in the inset (open circles), along with the corresponding exponents of the (002) peaks (solid circles).

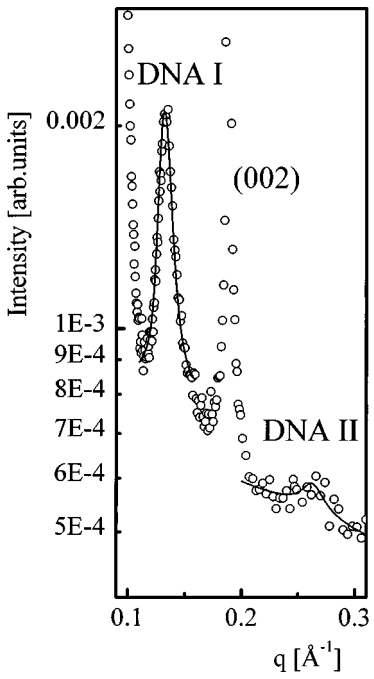

FIG. 6. In the $\nu = 1.5$ sample, a weak maximum is observed at the position of the second DNA harmonic. Apart from peak scaling and background, the simulation (solid lines) is to the same parameters as the fit of the fundamental peak (see Sec. III).

$\ll 1$, experimental real structure effects such as deviations from a perfect powder may spoil the applicability of the model and explain the deviations with respect to the theoretic prediction [24]. However, the powderlike nature of the complex suspensions was unambiguously evidenced by the Scherrer lines on an image plate detector. In the same manner, finite resolution and finite size are more critical experimentally for small η_m [25] and may account for deviations from the Caillé line shape. However, the resolution function was decaying much faster than the observed lamellar tails and deviations from Caillé's model are also found for the (002) peak, which is usually much less sensitive since η_m is expected to scale quadratically with the peak order. Here, this is clearly not the case, e.g., in the case of the $\nu = 1.5$ sample we find $\gamma = 1.55$ for the (001) and 1.29 for the (002) peak, respectively. We can thus safely attribute the observed deviations of the lamellar line shape to a more fundamental difference in the Hamiltonian of the complex phase from that of the conventional one. In particular, one has to bear in mind that the DNA strands lead to an enhanced stiffness of the lamellar system along the strand direction. This anisotropy of an effective membrane bending rigidity (at least on small length scales smaller than the DNA persistence length) cannot be captured by Caillé's model. Accordingly, the deviations must increase with DNA content as observed.

Presently, without any theories at hand, we cannot further analyze the scattering distribution of the lamellar peaks, and we turn directly to the analysis of the DNA correlation peak to gain insight into the nature of the DNA ordering in the complex.

The widths of the DNA correlation peaks range between 0.013 Å^{-1} and 0.023 Å^{-1}. This implies that positional correlations persist over roughly 5 to 10 times the interhelical spacing d. However, the DNA cannot be ordered in a perfect 1D lattice with parallel strands that fluctuate around well defined positions. Ignoring for the moment the finite bending stiffness with the resulting loss of positional correlations along the strands, a 1D solidlike model is contradicted by the absence of strong higher harmonics of the DNA correlation peak. In fact, estimating the Debye-Waller factor, e.g., for sample $\nu = 1.5$ from the ratio of the DNA correlation peak and the small bump that can be identified as its second harmonic, see Fig. 6, one would obtain a rms deviation of the strands with respect to their 1D lattice site of 0.4 d. At this level of fluctuation, no long-range order can persist. Furthermore, the line shape of the powder-averaged 1D solidlike model does not fit the data well in the tails of the peak, as will be shown in the next section. Thus, we can conclude fom the scattering distribution that there is no long-range order between DNA strands. This conclusion can of course also be drawn on fundamental grounds that a long-range ordered phase cannot exist in 1D [26].

More appropriately, the ordering of the DNA has to be described in a two-dimensional model, since the DNA strands cannot be treated as stiff and parallel rods. At least on length scales larger than the persistence length l_p, such an approximation has to break down, as orientational order along the stands (x direction in the local coordinate system)

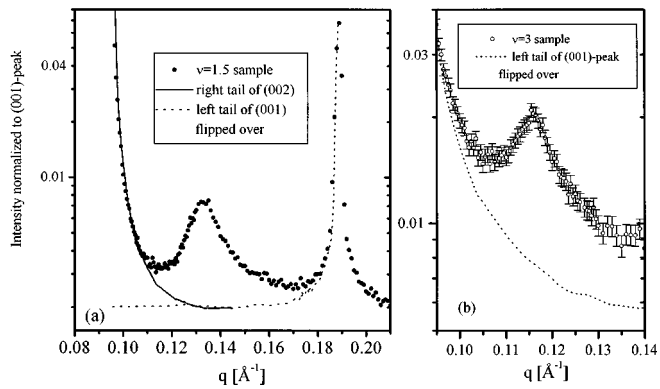

FIG. 7. (a) DNA correlation peak of sample $\nu=1.5$ with tails of the lamellar peaks on each side. To subtract the background, the unaffected left tail of (001) and right tail of (002) are flipped over (solid and dotted lines, respectively). (b) The same for the $\nu=3$ sample, where the DNA peak is riding on the right tail of the (001) peak.

will decay. Positional correlations due to small length scale fluctuations may vanish on even smaller length scales $l \ll l_p$. Additionally, if correlations between the DNA exist also across the lipid membrane (y direction in the local coordinate system), a correct model would have to be formulated in three dimensions. In the next section, we will show that the data are fitted well to the structure factor of a 2D smectic liquid crystal with additional short-range correlations across the lipid membrane, which can be regarded as a small pertubation of a purely 2D system. For low ν, these *cross correlations* vanish and the system becomes strictly two-dimensional.

Before exploring quantitative modeling in the next section, the issue of background subtraction must be discussed. For curves of medium L/D ratio where the DNA correlation peak lies in between the lamellar peaks, the background is fairly uniform with only little deviations from a constant value towards the tails of the lamellar peaks. A subtraction of the background without free parameters was carried out by the following procedure: The peak centers $q=lq_0$ of the $(00l)$ peaks were used as mirror lines for the unaffected tails of the opposite sides, which could then be inverted and subtracted without introducing further parameters. This scheme relies on the general observation that all the lamellar peaks are symmetric. Figure 7(a) shows the case of the $\nu=1.5$ sample (open circles) with the solid line representing the left tail of the (001) peak flipped over to the right side. For low q good overlap with the right tail is observed until deviations set in corresponding to the left tail of the DNA peak. The equivalent has been done with the tails of the (002) peak (dotted line). It is remarkable that the level of background of the two inverted tails coincides in the central q region. This nearly flat background scatter must also be attributed to the complexes, since the pure water scan results in scattering that is smaller by more than a factor of 2 in this q range. For samples of higher lipid dilution ν, the influence of the (001) becomes very dominant, but can still be taken into account in a similar manner by subtraction of the inverted left tail of the first lamellar peak. The situation is illustrated in Fig. 7(b) for the $\nu=3$ case. The most critical samples are those of low ν, where the (002) peak overlaps with the DNA peak. Since the latter is much broader, we decided to discard the data points corresponding to a strong (002) contribution and used the remaining data for the subsequent fitting, with correspondingly larger errors; see the following sections.

IV. FITS TO THE STRUCTURE FACTOR OF A 2D SMECTIC LIQUID CRYSTAL

The free energy density of a 2D smectic liquid crystal is given by

$$H/A=\frac{1}{2}B\left(\frac{\partial u(x,z)}{\partial z}\right)^2+\frac{1}{2}K\left(\frac{\partial^2 u(x,z)}{\partial x^2}\right)^2, \tag{2}$$

where $u(x,z)$ is a continuum displacement field of the DNA strands with respect to a perfect lattice in the local coordinate system defined in Fig. 1. B and K are the bulk moduli for strand compression (J/m^2) and strand curvature (J), with K related to the bending modulus of a single strand according to $K=K_s/d$. The corresponding free energy density for the Fourier component $\mathbf{q}$ is given by

$$F=\frac{1}{2}(Bq_z^2+Kq_x^4)u^2(\mathbf{q}). \tag{3}$$

Additional terms describing the coupling of the 2D-DNA phase to membrane undulations, i.e., the coupling between fluctuations of the nested 2D smectic and the 3D smectic ''host'' structure, may be neglected for membranes with high bending rigidity $K_m \gg k_BT$. Rigorous theoretic treatments of the free energy density containing also coupling terms have been developed independently by O'Hern and Lubensky as well as Golubović and Golubović [5,6]. However, it seems that the scaling behavior of the nested 2D smectic liquid crystal is not altered by the lamellar fluctuations of the 3D host fluctuations, thus justifying the simplistic approach of a rigid lamellar host structure. Furthermore, the very interesting effects arising from nonlinear elasticity theory and interlayer coupling become relevant only for length scales larger than those found in this experimental work. Equation (2) differs from the Hamiltonian of many previously studied 2D systems such as stripe-phase domain walls or step edges on crystal surfaces in that there is no line tension term [27], so that form fluctuations are governed by bending rigidity alone.

It is instructive to compute the mean-square fluctuation $\langle u^2\rangle$ by applying the equipartition theorem to Eq. (2),

$$\begin{aligned}\langle u^2\rangle &= \frac{kT}{(2\pi)^2}\int_{-q_0}^{q_{\max}} dq_z 2\int_{q_{\min}}^{q_{\max}} dq_x (Bq_z^2+Kq_x^4)^{-1} \\ &= \frac{2k_BT}{(2\pi)^2}\int_{q_{\min}}^{q_{\max}} dq_x 2\frac{\arctan(\sqrt{B/K}q_0/q_x^2)}{\sqrt{BK}q_x^2} \\ &\overset{q_{\min}\to 0}{=} \frac{k_BT}{2\pi\sqrt{BK}q_{\min}} = \frac{kTL_x}{(2\pi)^2\sqrt{BK}},\end{aligned} \tag{4}$$

where the integrals have been performed with MATHEMATICA [28]. Thus, $\langle u^2\rangle$ diverges linearly with the lateral system size L_x, which has to be compared to the $\langle u^2\rangle \propto L^3$ behavior of a

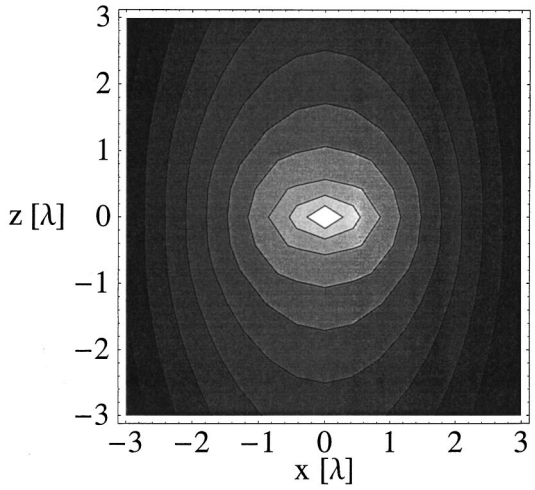

FIG. 8. The contour plot (logarithmic shading) of the correlation function $g(x,z)$ with x and z in units of λ at $\eta=0.08$.

single curvature governed polymer. The effect of the harmonic coupling between strands effectively reduces the divergence of $\langle u^2\rangle$. The resulting power law is the same as that of a single flexible polymer in 2D governed by surface tension rather than curvature. This also means that in contrast to the single chain result, the orientational order of the polymer confined in the stack becomes long-ranged. The correlation function $g(x,z):=\langle \exp(iq_0[u(x,z)-u(0,0)])\rangle$ is calculated from Eq. (3.1) in Appendix A, yielding

$$g(x,z)=\exp\left[-\eta\frac{2\pi}{\lambda}\sqrt{\pi\lambda|z|}\;\; e^{-x^2/(4\lambda|z|)} - \eta\frac{\pi^2}{\lambda}|x|\,\mathrm{erf}\left(\frac{|x|}{2\sqrt{\lambda|z|}}\right)\right], \tag{5}$$

with constants $\lambda:=\sqrt{K/B}$ and $\eta:=kTq_0^2/(2\pi)^2B$, and $\mathrm{erf}(z)$ denoting the error function [30]. Parallel to the strands, the correlation function decays exponentially $g(x,z\to 0)=\exp[-|x|/\xi_x]$ with a corresponding correlation length $\xi_x=\lambda/\eta\pi^2$. Normal to the strands, the correlations decay as $g(x\to 0,z)=\exp[\sqrt{z/\xi_z}]$, with $\xi_z=\lambda/(2\pi\eta)^2\pi$.

This result is noteworthy. Along the DNA strands the positional order decays exponentially in contrast to the algebraic decay of the 3D membrane counterpart. Normal to the strands, the decay is also much stronger than algebraic but still weaker than the liquidlike exponential decay that would apply, i.e., for harmonically coupled stiff rods or plates ($K=0$). Instead, the exponent z/ξ_z is replaced by $\sqrt{z/\xi_z}$, leading to a steep initial decay of correlations with z followed by elevated tails for larger z. This effect is visualized by the eye-shaped contour plot of $g(x,z)$ in Fig. 8. In this sense the 2D smectic liquid crystal is a unique liquid crystalline state of matter.

The structure factor of a single-domain sample is obtained by Fourier transforming in the variable (q_z-q_0,q_x). Along the q_x axis the peak is a simple Lorentzian (HWHM $=1/\xi_x$), but along q_z it exhibits a singularity with tails that decay to lowest order like $q^{-3/2}$ for $q\gg 1/\xi_z$. Analogous to the power-law singularities of 2D crystals and stacked membranes, a finite size factor is introduced [29], that accounts for a broadening of the central peak to a finite domain size L. Since the data were taken from perfectly isotropic suspensions, the ''single crystal'' result then has to be ''powder-averaged'' in three dimensions. First, the structure factor is averaged in the two-dimensional q_x/q_z space over the angle ϕ between the average helical axis of the DNA and the x axis, resulting in an expression that is applicable when the DNA is powderlike but the membrane stacks are perfectly oriented,

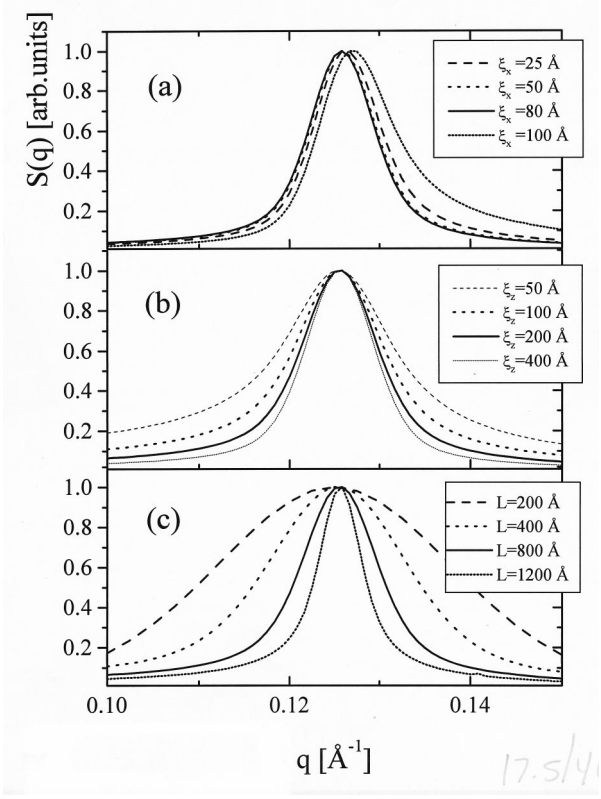

FIG. 9. The 2D smectic line shape after in-plane powder averaging: (a) varying ξ_x at constant $\xi_z=200$ Å and $L=900$ Å; (b) varying ξ_z at constant $\xi_x=400$ Å and $L=800$ Å; (c) varying L at constant $\xi_z=200$ Å and $\xi_x=400$ Å.

$$S_{2D}(q_{xz})=\frac{1}{2\pi}\int_{-\pi}^{\pi}d\phi\int_{-\infty}^{\infty}dx \times\int_{-\infty}^{\infty}dz\; g(x,z)e^{-r^2\pi/L}e^{-i(\mathbf{q}-\mathbf{G})\cdot\mathbf{r}}. \tag{6}$$

Here, $\mathbf{q}=(q_x,q_y)$, $\mathbf{r}=(x,z)$, and $\mathbf{G}=q_0\hat{z}=2\pi/d\hat{z}$. Investigating the resulting line shapes one finds that curves of fixed ξ_z and L become independent of ξ_x (apart from an absolute scaling factor) if ξ_x becomes larger than d; see Fig. 9. In other words, in this limit the line shape is the same as that of an equivalent ensemble of rigid rods fluctuating only in their positions along z. Since the DNA is known to be quite stiff, it is therefore not surprising that only ξ_z can be extracted from the fitting, in the same manner that the bending rigidity K_m cannot be determined for stiff membranes [17].

Next, the membrane normal is summed in 3D over all configurations with respect to **q**,

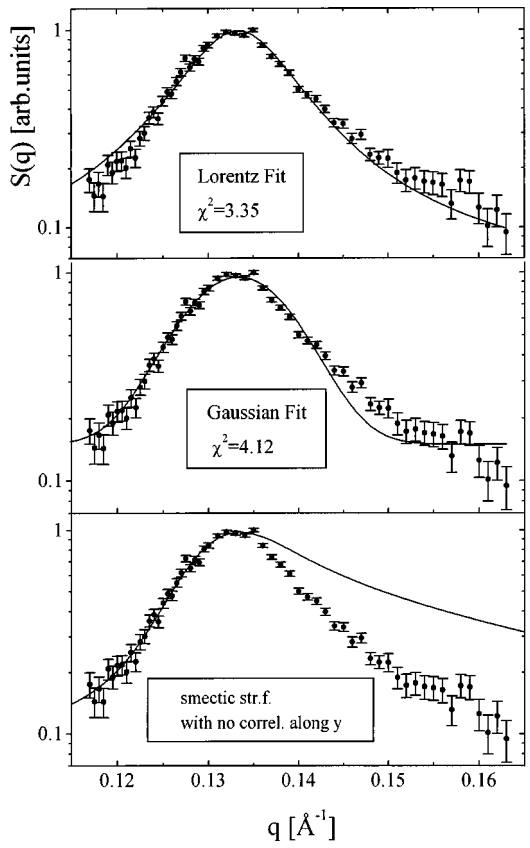

FIG. 10. Fit of (a) Lorentzian and (b) Gaussian line shapes to the DNA peak of sample $\nu=1.5$. Obviously, these simple empirical line shapes fail to explain the data, and a more rigorous modeling is required. (c) Simulation of 2D smectic correlation with no positional correlations of the DNA across different layers, yielding a right slope that is systematically too high.

$$S_{3D}(q) \propto \int_{-\pi/2}^{\pi/2} d\theta \, \sin(\theta) S_{2D}(q \, \sin\theta) \times \left(\frac{J_1(r_D q \cos\theta)}{r_D q \cos\theta} \right)^2 f_y(q \, \cos\theta). \qquad (7)$$

The second factor in the integrand is the cylindrical form factor of DNA with radius $r_D=11$ Å. The form factor appears only here rather than already in Eq. (6), because it can be shown numerically that it does not affect the 2D powder average if the correlation length ξ_z is large compared with the DNA radius r_D. Contrarily, it must be included in the present step of the 3D powder averaging, if the DNA strands are not correlated over a long range along y, i.e., across the layers. A long-range correlation in this direction would imply the existence of additional peaks in the powder spectrum, which are not observed. $f_y(q_y)$ is the structure factor of the truncation rod, which is constant for a true 2D system, i.e., also for perfectly uncorrelated layers . However, $f_y=1$ does not fit the data with the right tail of the simulated peak being systematically too high; see Fig. 10(c). In other words, the model of perfectly flat and uncorrelated planes of DNA cannot explain all the data. We therefore introduce a decaying structure factor that for the sake of simplicity is taken to be of one of the two following simple forms:

$$f_1(q_y) = \frac{1}{\xi_y^2 + q_y^2}, \quad f_2(q_y) = \exp[-(\sigma q_y)^2], \qquad (8)$$

with f_1 corresponding to an exponential correlation across different layers with a decay length ξ_y, and f_2 corresponding to a damping due to height fluctuations of amplitude σ. Beforehand, we knew that ξ_y must be of the same order as d_m, since if it was larger, extra peaks of 2D ordering of the DNA strands (e.g., on a hexagonal or rectangular lattice) would have to appear; see above. Alternatively, f_2 is appropriate for an uncorrelated but strongly fluctuating system, where the fluctuations of the DNA and lipid sheets in the y direction would give rise to such a Debye-Waller term. The fitting results in this case vary between $\sigma=0.3$ d and $\sigma=0.4$ d, where σ corresponds to the fluctuation amplitude on the lateral length scale of the DNA domain L_x, i.e., typically a few hundred Å. These high values are incompatible with the existence of higher harmonics of lamellar peaks, e.g., the (002) peak that is observed throughout, typically weaker than (001) by one order of magnitude. More drastically, at $\sigma/d_l \simeq 0.3$ the fourth harmonic (004) observed in the $\nu=1.5$ sample should be weaker than (001) by about 23 orders of magnitude. By estimating the rms deviations to be around $\sigma \simeq 10$ Å, consistent with the intensity ratios of the higher harmonics, we can safely rule out this model, and accept the existence of weak short-range cross correlations between the DNA strands of neighboring layers as the valid effect, even if least-square fitting leads to similar χ^2 values for either form. Recent theoretical studies on DNA-lipid complexes predict a ''new phase'' of vanishing positional and persisting orientational cross correlations, i.e., an orientational but no positional coupling between DNA strands of different layers [5,6]. This does not mean, however, that there are no short-range positional correlations. Indeed, the ''sliding columnar phase'' predicted by the studies also implies an exponential decay along y of the positional cross correlations, i.e., just as is assumed for the line shape fitting in this work [first term in Eq. (8)] [5]. Moreover, the 3D smectic undulations of the lipid membrane ''host structure'' were shown to have no qualitative effect on the DNA ordering, i.e., on the functional behavior of $g(x,z)$ [6].

Figure 11 shows the fits of the data to Eq. (6) with f_1 in Eq. (7) as the rod function, where the fitting has been carried out on a pentium PC platform with a software package of nonlinear and evolutionary fitting algorithms [31]. Seven peaks with least-squares fits are displayed, corresponding to samples of $\nu=0$, 0.35, 0.67, 1, 1.5, 2.33, and 3 [curves (a) through (g)], with respective least-squares deviations χ typically around 1.5 per degree of freedom. The curves are plotted as a function of the normalized wave vector $(q-q_0)/q_0$, and have been shifted by additive constants along the abcissa for better comparison. In curves (a) and (b) the lamellar (002) peak falls on the left slope of the DNA correlation peak so that the affected data points had to be removed, resulting in larger fitting uncertainties. The fitting parameters of the model were ξ_z, ξ_y, L, d as well as a scaling factor and a constant background level that was allowed to vary in a range of a few percent of the peak maximum to account for small possible errors in the previous background subtraction. ξ_x was kept constant in the range where it does

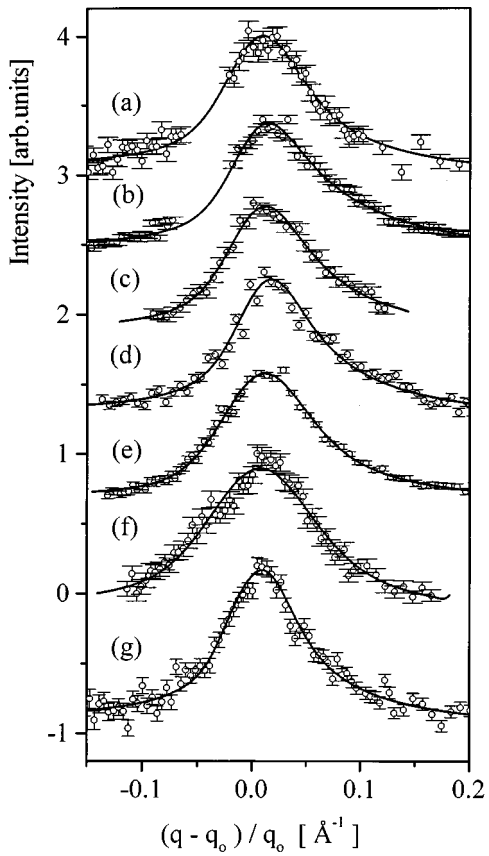

FIG. 11. Normalized and rescaled DNA correlation peaks after background subtraction and the corresponding fits to 2D smectic line shape [Eqs. (6) and (7)] for samples $\nu=0$, 0.35, 0.67, 1, 1.5, 2.33, and 3 [curves (a) through (g)].

not affect the lineshape $\xi_x \gg 2d$; see above. In the simulations, L is found to be inversely proportional to the Gaussian-like center of the curve. Changes of ξ_z are most visible in the left tail where the scattering gets weaker with increasing ξ_z resulting in a steeper left slope. The right tail was dominated by the value of ξ_y, which can be understood in geometrical terms, since the truncation rods are tangents to the Ewald sphere and intersect at $q>q_0$. The striking asymmetric profile observed, in particular, for samples of medium ν ratio, occurs when the correlation length ξ_z is relatively large, leading to a steep left tail, but ξ_y is still relatively small, leading to a slowly decaying right tail. The fitting results of all samples are displayed in Table I and will be discussed in the next section.

As described above, the low-dimensional nature of the self-assembly is directly apparent in the powder-averaged scattering profile, and models with different geometries (e.g., 2D hexagonal phase, 3D nematic, etc.) fail to explain the data. However, within the given geometry of DNA ordered as parallel strands in a two-dimensional plane, different models with relatively small variations in the correlation function along z are harder to differentiate by the line shape analysis, since small domain sizes and powder-averaging effects somewhat blur the distinct features of each model. To investigate this issue, alternate models were fitted assuming true solidlike and liquidlike ordering of parallel DNA strands, respectively. The latter case corresponds to the line shape of a 2D nematic liquid crystal composed of stiff polymers like

TABLE I. The fitting results: the first three rows correspond to the results of the 2D smectic model fitting to Eq. (6), with either $f_1(q_y)$ (parameter ξ_y) or $f_2(q_y)$ (parameter σ), respectively, as the rod function in Eq. (7). The last row gives the results of the correlation length ξ when fitting to a 2D nematic (1D liquid) model.

sample $\nu=$	0	0.35	0.67	1	1.5	1.94	2.33	3
d (Å)	27.6	28.7	38.1	39.9	47.9	52.4	53.0	54.7
L (Å)	475	539	667	895	634	521	602	1080
ξ_z (Å)	91	108	141	131	311	189	148	176
ξ_y (Å)	20	10	24	33	31		60	52
σ (Å)	9.2	8.5	14	13.5	18		26	24
ξ (Å)	103	113	167	168	183		173	212

DNA. The χ^2 values of the corresponding curves were generally higher than for the smectic liquid crystal model. The situation is illustrated in Fig. 12 for the case of the sample $\nu=1.5$, with the 1D solid structure factor (1D Gaussian, powder averaged in 3D as described above) resulting in a least-squares deviation of $\chi^2_{\mathrm{sol}}=2.2$, and the 1D liquid structure factor (1D Lorentzian, powder averaged in 3D as described above) in a value of $\chi^2_{\mathrm{liq}}=1.95$, as compared to $\chi^2=1.65$ for the smectic liquid crystal model. But even without referring to these somewhat small differences, 1D solidlike ordering can be ruled out because higher harmonics would be much stronger in this case; see the preceding section. The

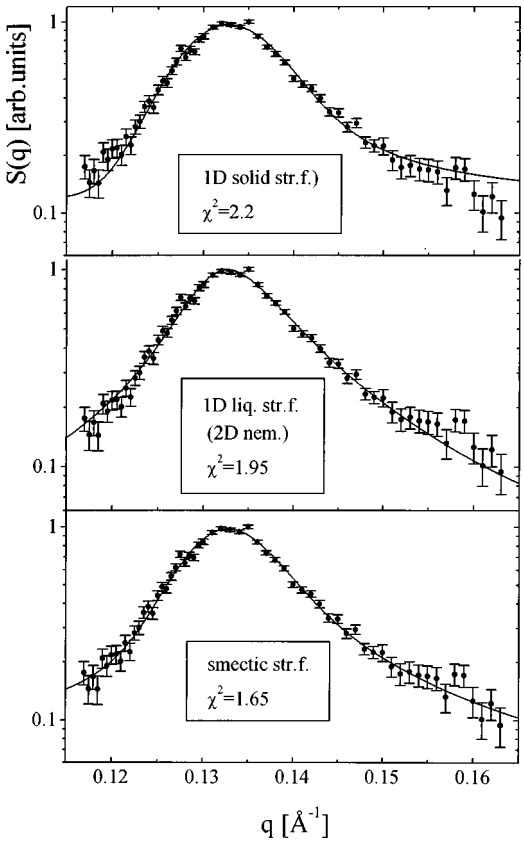

FIG. 12. DNA peak of the $\nu=1.5$ sample with (a) a 1D solid, (b) a 1D liquid (2D nematic), and (c) a 2D smectic line shape. The 3D powder averaging scheme with an exponential correlation function along y was the same for all three fits. Small but statistically significant differences are observed in the tails.

2D nematic model, on the other hand, requires untypically high values for the correlation lengths perpendicular to the strands of the order of four to five lattice units. To this end, a 2D smectic phase and a highly correlated 2D liquid of polyelectrolyte strands cannot be distinguished very well by the line-shape analysis, but the latter can be rejected on the basis of the fitting results. Theoretically, the two phases become equivalent on long length scales, due to dislocation defects that are free in 2D [32]. Indeed, a high defect density in the complexes is also obvious from the small values of smectic domain sizes L inferred from the fitting. Interestingly, defects have also been imaged by atomic-force microscopy (AFM) in fingerprintlike patterns of DNA adsorbed to lipid bilayers [33]. This system, however, differs from the present one in that it is constrained by the presence of a substrate and it is composed only of one bilayer covered with DNA rather than a multilamellar structure with the DNA sandwiched in between two bilayers. Moreover, for the AFM images the lipid is required to be in the gel phase with ordered tails in contrast to the liquid nature of membranes in the complexes. However, the ordering of DNA strands is most probably also of smectic symmetry.

Finally, we justify the use of the harmonic approximation *a posteriori* by the relative values of the smectic domain sizes ξ_z and ξ_x obtained in the present work (called dislocation length in [19]). Nonlinear effects become observable only when ξ_x and ξ_z become larger than the respective Ginzburg length ξ_{Gx} and ξ_{Gz}, which are given in 2D by [19]

$$\xi_{Gx}=\frac{8\pi(K/k_BT)^{3/2}}{(B/k_BT)^{1/2}}, \quad \xi_{Gz}=\frac{\xi_{Gx}^2}{\lambda}. \tag{9}$$

From the results of the fitting we only get a combination of K and B (or alternatively λ and η, or ξ_x and ξ_z, see the definitions above), so that we cannot evaluate the Ginzburg lengths directly. However, as will be discussed in the next section, the bending rigidity can be related to the persistence length ξ_p of DNA according to $K=k_BT\xi_p/2d$, which allows us to remove this ambiguity and calculate the quantities above to $\xi_{Gx}\simeq 0.7$ μm and $\xi_{Gz}\simeq 80$ μm. These values are much higher than those found experimentally for ξ_x and ξ_z; see the next section. Accordingly, nonlinear terms in the Hamiltonian are irrelevant and the interesting theoretic relationship [19] between a 2D smectic liquid crystal and the KPZ theory of a growing interface (growth in D=1+1, with one substrate dimension), which has been mentioned in the Introduction, must in this case be drawn as an analogy to the linear version of the KPZ equation, the so-called Edwards-Wilkinson (EW) equation [34]. The EW equation has been used in many different linear theories of interfacial evolution as well as in corresponding computer simulations. Furthermore, it has been verified experimentally to apply to the interface evolution of sputter-deposited amorphous multilayers (in D=2+1) [35]. In the picture of the analogy, the z axis of the 2D smectic liquid crystal would be mapped to the time axis of the interface evolution, while x would be the spatial coordinate. Interface fluctuations of different smectic layers (strands) would then correspond to interface positions of subsequent points in time in the stationary growth regime, with the EW coefficient proportional to $k_BT/\sqrt{BK}$. Indeed, for D=1+1 the equation predicts the same divergence of $\langle u^2\rangle$ with the lateral system size as Eq. (3).

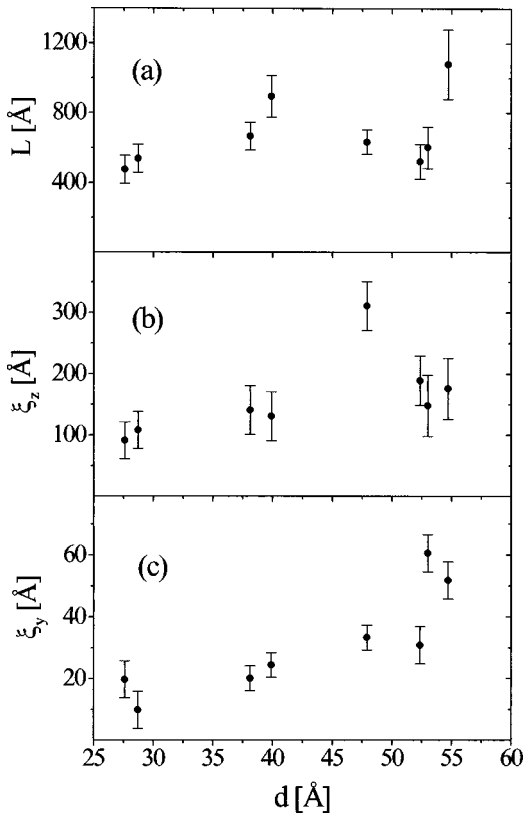

FIG. 13. The results of the least-square fitting: (a) DNA smectic domain size L, (b) correlation length ξ_z, and (c) correlation length ξ_y perpendicular to the layers, as a function of DNA spacing.

V. FITTING RESULTS AND MICROSCOPIC INTERACTIONS

The results for L, ξ_z, and ξ_y obtained from fitting the data to Eq. (6) with rod function $f_1(q_y)$ in Eq. (7) are shown in Table I. The second to last row contains the Gaussian width σ, as obtained by using the alternative rod function $f_2(q_y)$. As discussed in the preceding section, an increasing width of the 2D layers could only be explained by a strongly fluctuating multilayer, and by inspection of the values the model can be ruled out, since it is inconsistent with the strong second harmonic of the lamellar peaks; see above. The fitting results for L and ξ_z obtained with $f_2(q_y)$ and $f_1(q_y)$ fall within the respective error bars. The values for d are shifted by about 0.2 Å when using $f_2(q_y)$ instead of $f_1(q_y)$. Finally, the last row of the table gives the values of the liquid correlation length as obtained from the 1D liquid (2D nematic) structure factor. Again, the model can be ruled out on the basis of the unrealistically high correlation lengths and also the slightly higher χ^2 values, e.g., see Fig. 12(b).

Therefore, the 2D smectic ordering with weak exponential correlations along y can be established as the valid model. In Fig. 13 the corresponding values of L, ξ_z, and ξ_y are plotted versus d. L is found to vary nonsystematically between 500 Å and 1200 Å, see Fig. 13(a), while Fig. 13(b) shows a moderate overall increase of ξ_z with d. The highest value of $\xi_z=311$ Å is determined for the $\nu=1.5$ sample. Expressed

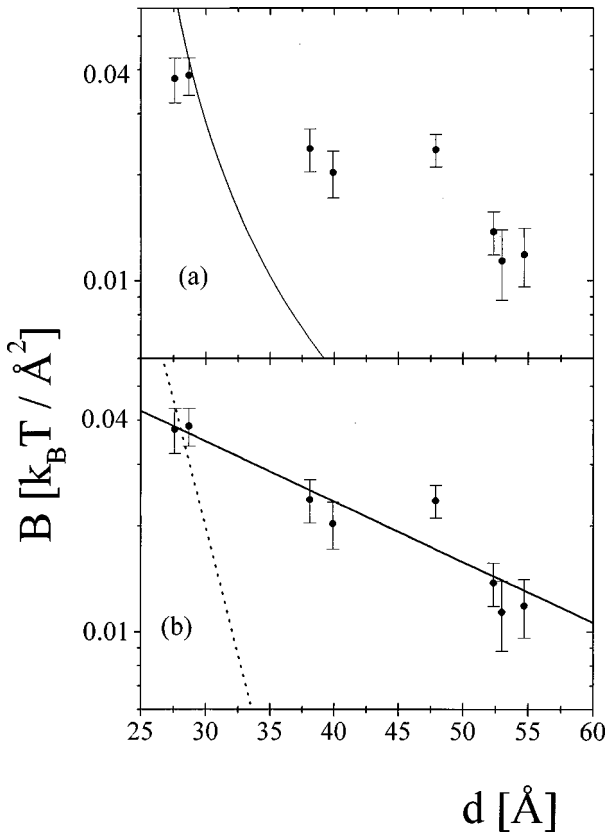

FIG. 14. The compressional modulus B in units of $k_BT/\text{Å}^2$ as a function of d on double-logarithmic scale. The data points as extracted from the fitting (see text) are the same in (a) and (b), but plotted versus the predictions for different microscopic interactions: (a) Helfrich steric repulsion (solid line), (b) exponential interaction $B \propto \exp[-d/l]$ as resulting from hydration forces or screened electrostatics, respectively, with $l=3$ Å (dotted line) and 25 Å (solid line). Hydration interaction could only explain the very first data points, and screened electrostatics can be discarded since the Debye length λ_D is several hundred Å in the present case, and thus much larger than the 25 Å obtained from the fit.

in lattice units, this flat dependence translates into a significant decay of the correlation length with d. Using the definitions of ξ_z and ξ_x given in the preceding section, one can extract the 2D chain-chain compressional modulus B,

$$B=(2\pi)^2 2^{-2/3}\frac{(k_BT)^{4/3}}{K^{1/3}}\left(\frac{\xi_z}{d}\right)^{2/3}\frac{1}{d^2}. \tag{10}$$

We can now proceed by estimating the bending rigidity (or splay modulus) K. As a reasonable assumption, K can be linked to the single DNA bending rigidity K_s by $K=K_s/d$, with K_s in turn being proportional to the DNA chain persistence length $\xi_p=2K_s/k_BT$ [36], which has been experimentally measured to be $l_p \simeq 500$ Å [11]. The corresponding values are plotted in Fig. 14 for $\xi_p=500$ Å. Different values of ξ_p merely change the curve by a multiplicative factor, but not the d dependence. Of course, the analysis of the results is severely limited by the small number of points and the relatively large error bars. Refined data will become available in time with ongoing studies, and possibly also from oriented samples. However, to this end the experimental curve $B(d)$ can be compared to various different models, from which significant conclusions can be drawn.

(a) Let us consider if steric repulsion of the DNA strands may be responsible for the ordering, analogous to the steric interactions in membrane systems [17], which were theoretically proposed by Helfrich [37]. However, this would imply considerable strand undulations on lateral length scales of the order of d, with a corresponding line shape significantly different from the one observed, which is consistent with undulations only on longer length scales. Thus, we conclude that steric undulations are irrelevant in the present case. Independent of the line-shape argument, Helfrich's interaction can be clearly ruled out from the measured $B(d)$ dependence. Following Helfrich [38], the mean square of the displacement u for a polymer of length l in a two-dimensional plane is $\langle u^2\rangle = k_BTl^3/2K_s$, where K_s is the bending rigidity of the polymer. The mean number of contacts per unit length of a polymer confined between walls of separation d or in a corresponding array of parallel polymer chains is therefore given by $1/l_H$, with a collision length of $l_H = (d^2 2K_s/k_BT)^{1/3}$. An entropic free energy cost of k_BT can be attributed to each collision, so that the free energy per surface area is given by

$$\frac{F}{dl_H}=\frac{k_BT(k_BT)^{1/3}}{(2K_s)^{1/3}d^{5/3}}. \tag{11}$$

From the definition of the compressional modulus as the second derivative of the free energy density $B = d^2\partial^2(F/A)/(\partial d)^2$, we get for Helfrich's interaction

$$B=\frac{40}{9}\frac{k_BT}{\xi_p^{1/3}}\frac{1}{d^{5/3}}, \tag{12}$$

where K_s has again been expressed in terms of the known persistence length ξ_p. The corresponding form is plotted as the solid line in Fig. 14(a) for $l_p=500$ Å, and corrected for the finite size effect, i.e., by replacing d by $d-r_D$ [39]. A similar result with a different prefactor has been derived for hexagonal phases of polymers [40]. Clearly, this curve does not fit, and this remains to be the case also when the prefactor is treated as a fit parameter, which is appropriate, since only a more rigorous derivation can yield a correct value of the prefactor [41].

(b) Hexagonal phases of DNA have been extensively studied by osmotic pressure techniques for different salt concentrations [42,43]. At high DNA densities corresponding to interhelical distances of up to about $d=30$ Å, hydration interaction dominates, giving rise to an exponentially decaying repulsive force per unit length of DNA,

$$f_h(r)=f_{h0}e^{-(d-2r_D)/\lambda_h}, \tag{13}$$

with typically $f_{h0}=90$ dyn/cm and $\lambda=3.1-3.5$ Å [42]. In the same way, the DNA packed in the complexes can be expected to experience a strong contribution of hydration forces at small $d \leqslant 30$ Å. The corresponding curve of the compressional modulus $B(d) \propto \exp(-d/3\ \text{Å})$ is plotted in Fig. 14(b). Clearly, hydration alone cannot account for the experimental data over the whole range of d.

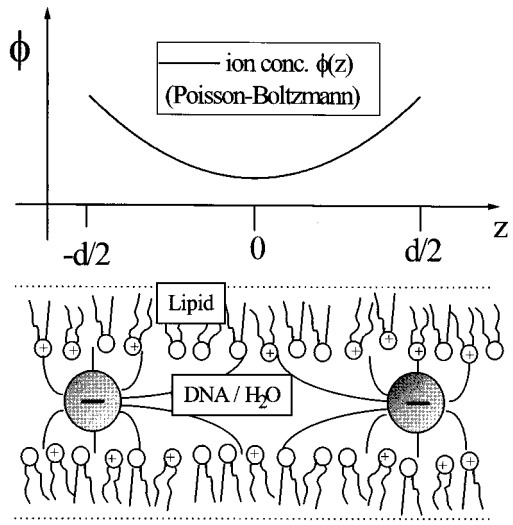

FIG. 15. Schematic of the DNA and the corresponding counterions of cationic lipids (DOTAP) in the lipid bilayers composed of DOPC/DOTAP. The concentration profile of the DOTAP counterions is sketched above the bilayer.

In the regime of interhelical distances 30 Å$\leqslant d \leqslant$120 Å, pure solutions of DNA in brine exhibit an electrostatic interaction screened by the salt ions, leading to an exponential decay of the repulsive forces. Fitting the data to an exponential decay of arbitrary range l, $B \propto \exp[-r/l]$, agreement can be obtained only for $l \simeq 25$ Å; see the solid curve in Fig. 14(b). The corresponding salt concentration of 14.4 mMol is, however, much higher than in our samples. Indeed, preparing the samples with ultrapure water (Millipore), the ion concentration is given by only the anions corresponding to the cationic lipid and the cations corresponding to the DNA, which get fully released when the DNA and the lipid condense. This increase in free ions and the corresponding gain in entropy is the driving force of the self-assembly. However, the ions are released into the full volume of excess water in the capillary, resulting in a relatively low concentration, which can be estimated to be below 1 mM. Further experimental proof is of course given by the fact that the DNA dilutes to above 60 Å (where this number is not limited by electrostatics but by lipid phase separation), giving an upper bound for the concentration of salt of about 2.5 mM. A fit to an exponential curve $B(d)$ with $l=60$ Å is, however, in complete disagreement with the data. Thus, we conclude that in contrast to pure DNA solutions, electrostatic interaction screened by salt cannot account for the DNA ordering in the complexes.

(c) The interactions may thus be attributed to a combination of hydration forces (at short range) and long-ranged electrostatic forces. In the limiting case of infinitely high mixing enthalpy of the cationic lipid and the neutral colipid, or, equivalently, in the special case of no neutral colipid ($\nu=0$), the system could be approximatively treated as an assembly of oppositely charged planes and lines; see Appendix B. For $\nu \neq 0$, the system has to be described self-consistently by the Poisson-Boltzmann equation just as in the well known case of stacked membranes [45]. However, the present geometry is somewhat more complicated, since the electric field distribution has to be parametrized in at least two dimensions. A 2D cross section with quantitative field lines is sketched in Fig. 15.

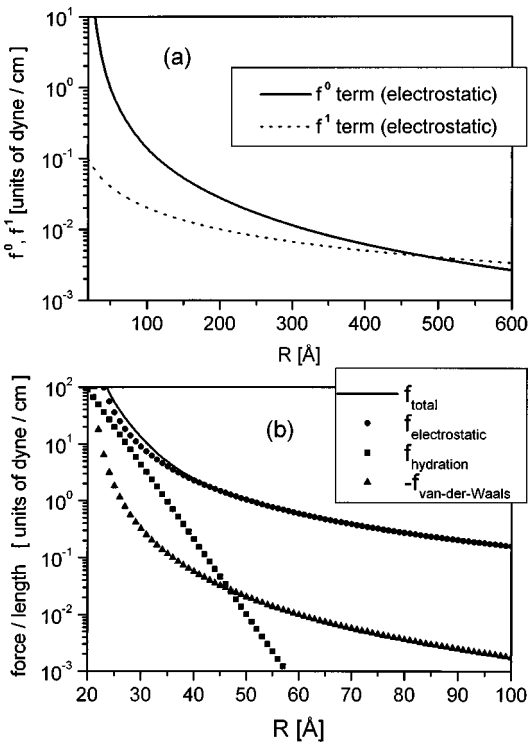

FIG. 16. The force laws of various microscopic interactions (force per unit length of DNA): (a) The two dominating terms of the solution of the Poisson-Boltzmann problem [4], (b) the contributions of the van der Waals force (attractive), hydration force, the Poisson-Boltzmann result (sum of f^0 and f^1), as well as the combination of all of the above. As can be seen, the van der Waals contribution is negligible over the entire range, while hydration forces become comparable to the electrostatic (Poisson-Boltzmann) term at small d.

Bruinsma and Marshl have addressed the problem [4] and obtain two main contributions for the repulsive force $f(d)$ per unit length,

$$f^0(d) \simeq \frac{\pi k_B T r_D}{2 l_B (d-\delta)^2}, \quad f^1(d) = 2\ln(2)\left(\frac{\epsilon_l}{\epsilon_w}\right)\frac{k_B T}{l_B d}, \quad (14)$$

which are due to the osmotic pressure of lipid counterions and long-range electrostatic forces, respectively, calculated by using the Maxwell stress tensor, i.e., considering the energy of the electric field between neighboring DNA chains. In these equations, l_b is the Bjerrum length in water $l_b = e^2/(\epsilon k_B T) = 7.1 \times 10^{-8}$ cm ($\epsilon_{\mathrm{H_2O}} = 78.5$, $\epsilon_{\mathrm{lipid}} = 2$), $r_D = 10^{-7}$ is the DNA radius, and Δ is a somewhat empirical distance below which the formula for f^0 does not work, roughly equal to the DNA radius. f^0 and f^1 are the lowest-order terms in an expansion of small r_D/r, so that the result is valid only for large DNA separations. The finite size is neglected, and the equation is not applicable for $\nu=0$ (pure cationic lipid, see Appendix B), where the osmotic pressure of lipid counterions vanishes. The two force contributions are shown in Fig. 16(a): $f^0 \propto 1/d^2$ dominates at small d, with a crossover at $d=483$ Å.

Let us also consider the van der Waals force between the DNA strands,

$$f_{\mathrm{vdW}} = -\frac{A\sqrt{r_d}}{16(d-2r_D)^{5/2}}, \tag{15}$$

where the Hamaker constant $A = 5.2\times 10^{-14}$ erg has been derived with $\epsilon_{\mathrm{DNA}} = 4$ and $\epsilon_{\mathrm{H_2O}} = 80$ [46]. This is an attractive force that is smaller than the previous two contributions, at least at very low ionic strengths. The electrostatic, hydration, (van der Waals), and the resulting total force are shown in Fig. 15(b) for the distances covered in the lipid dilution experiment. We see that electrostatic forces are dominant except at small r, where hydration forces are comparable.

To compare the above forces with the experimental $B(d)$ data, we need to calculate B and to convert it to the units of $k_BT/\text{Å}^2$. This is accomplished with the thermodynamic definition $B = d(\partial f/\partial d)$, where f is the force per unit length as used in the above formulas. Correspondingly, we obtain

$$B_{\mathrm{Poiss.\text{-}Boltz.}} = \frac{\pi k_B T r_D d}{l_B(d-2\Delta)^3} + 2\ln(2)\left(\frac{\epsilon_l}{\epsilon_{\mathrm{H_2O}}}\right)\frac{k_BT}{l_B d}, \tag{16}$$

$$B_{\mathrm{hydr}} = d\,\frac{f_{h0}}{\lambda_H} e^{-(d-2\Delta)\lambda_H}, \tag{17}$$

$$B_{\mathrm{vdW}} = \frac{5A\sqrt{r_D}}{32}\,\frac{d}{(d-2\Delta)^{7/2}}. \tag{18}$$

In the above formulas Δ, f_{h0}, and λ_h are fitting parameters, since they may be somewhat different in the DNA-lipid complexes than predicted or measured for bulk DNA phases. The comparison with the experimental data in Fig. 17(a) shows that the decay in $B(d)$ is slower than current thoeretical predictions. The solid curve in Fig. 17(a) is a fit to the data, restricting coefficients to be reasonable (positive and not larger than several Å in the case of Δ and λ_h). The values of the simulated curve are $\Delta = 9$ Å, $\lambda_h = 3.1$ Å, and $f_{h0} = 0.014 k_BT/\text{Å}^2$, all of which are very close to the ones given in the literature ($f_{h0} = 0.021 k_BT/\text{Å}^2$ in bulk DNA phases, but this difference is not significant, considering how poor the fit is). Thus, the conclusion can be drawn that the electrostatic prediction [4] is two large at small d and decays too quickly compared with the data. This is not too surprising considering the above discussion, where the work of Ref. [4] does not take into account that the lipid osmotic pressure should vanish as $d \to 2r_D$ with $\nu = 0$ (pure cationic lipid).

What can then be compared favorably with the data? Figure 16(b) shows a fit to a hypothetical $1/d$ dependence with added hydration and van der Waals contributions (solid line). The fit is to the sum of the respective terms $B = B_h + B_{\mathrm{vdW}} + C/d$, with B_h, B_{vdW}, and l_b the same as above and C as the coefficient of the $1/d$ term. As shown above, the B_{vdW} contribution is negligible, but has nevertheless been included here since it introduces no free parameters. The fit parameters were $C = 43.6$, $f_{h0} = 0.109$, and $\lambda_h = 3.23$ Å. We can draw a definite conclusion that hydration forces are important (improving the fit in a statistically significant way) at small d with a decay length of 3.2 Å, of about the same strength as in bulk DNA phases. At larger separations, the $1/d$ term dominates. Moreover, an additional $1/d^2$ term does not improve the fit. The $1/d$ decay of the electrostatic contribution may be related to a short calculation for the case of pure cationic lipid or no lipid demixing presented in Appendix B, suggesting that the simplest electrostatics without a Poisson-Boltzmann-like counterion pressure captures the essence of the DNA-DNA interaction in the complexes. The counterion pressure in this quasi-two-dimensional system with very large and relatively few ''solvent'' (neutral lipid) and ''counterion'' (cationic lipid) molecules may not be as relevant as in the ordinary three-dimensional analog of charged membranes. However, to safely draw conclusions on this issue, further theoretical calculations that are valid also in the experimentally important regime of small DNA spacings d are required.

Another possible contribution to the compressibility modulus B may arise from changes in ratio of the membrane area to lipid head group area, and the associated chain stretching. This mechanism assumes that the average area per lipid molecule is reduced rather than neutral lipids being expelled from the complex when the DNA distance is decreased. However, an estimate of the lipid compressibility shows that the contribution to B would be independent of d and of the order of $2k_BT/\text{Å}^2$.

All of the interactions discussed above, aside from the negligible van der Waals contribution, are purely repulsive. The average density and hence an average interhelical distance d is fixed by the condition of overall charge neutrality (isoelectric regime), with the repulsive interactions responsible for the ordering.

In summary, we have demonstrated that the DNA orders as a 2D smectic phase in the 3D smectic DNA/lipid complex, with the interhelical distance determined by the average bilayer charge density. The ordering is found to be inconsistent with pure hard-core interactions, steric repulsion, and hydration forces, but can be well explained by long-ranged electrostatic forces with the cationic lipids acting as counterions. Furthermore, the line-shape analysis shows that short-ranged positional cross correlations exist between the DNA of adjacent layers. For the samples of small d near close packing these cross correlations vanish, but they become very pronounced for samples of higher spacing ν, where the correlation length increases with interhelical spacing d. For the present work, the analysis was limited by the significant errors and the effects of powder-averaging. Further insight may be derived from studies of oriented samples that may become available in the future. The correlation of complex structure and fluctuations to properties such as synthetic gene carriers also remains to be explored.

ACKNOWLEDGMENTS

We acknowledge useful discussions with N. Dan, P. Pincus, B. Gelbart, T. Lubensky, F. MacKintosh, L. Golubović, and in particular, R. Bruinsma for communicating his electrostatic calculations. This work was supported by NSF-DMR-9624091, the Petroleum Research Fund (31352-AC7), and a Los Alamos CULAR grant STB/UC:96-108. T.S. would like to thank the DAAD for the distribution of a NATO grant. J.O.R. acknowledges a DFG grant (Ra 655/1-

1). The Materials Research Laboratory at Santa Barbara is supported by NSF-DMR-9632716. The synchrotron experiments were carried out at Stanford (SSRL) supported by the U.S. DOE.

APPENDIX A: CALCULATION OF THE CORRELATION FUNCTION

In continuum description the correlation function can be defined as

$$g(x,z)=\langle \exp\{iq_0[u(x,z)-u(0,0)]\}\rangle, \tag{A1}$$

where $q_0=2\pi/d$ is the q value corresponding to the first correlation peak, and $u(x,z)$ denotes the displacement of the DNA strands with respect to a perfect lattice in a local coordinate system. In the harmonic approximation valid for small displacement amplitudes, u is a Gaussian random variable, so that the ensemble average $\langle\ \rangle$ has to be performed only over u. Using Eq. (3) of Sec. III we are therefore left to evaluate

$$\langle \tfrac{1}{2}q_0^2|u(x,z)-u(0,0)|^2\rangle = \eta\int_{-\infty}^{\infty}dq_x\int_{-\infty}^{\infty}dq_z\frac{1-\cos[q_x x+q_z z]}{q_z^2+\lambda^2 q_x^4}, \tag{A2}$$

with η and λ as defined in Sec. III. Using the integral

$$\int_{-\infty}^{\infty}dx\frac{1-\cos[a(b-x)]}{x^2+c^2}=\frac{\pi}{c}(1-e^{-ac}\cos[ab]), \tag{A3}$$

which can be calculated, e.g., by MATHEMATICA [28] after switching to a complex representation of the cos function, the d_z integral is carried out, leading to

$$\langle \tfrac{1}{2}q_0^2|u(x,z)-u(0,0)|^2\rangle = \int_{-\infty}^{\infty}dq_x\frac{\pi}{\lambda q_x^2}(1-e^{-\lambda q_x^2 z}\cos[q_x x]). \tag{A4}$$

The remaining integral over q_x can be solved by partial integration rewriting the integrand as

$$f(Z,x)=f(0,x)+\int_0^Z dZ'\frac{\partial f}{\partial Z'}, \tag{A5}$$

with $Z=\lambda z$. For the integral corresponding to the first term on the right-hand side of Eq. (20) we get (MATHEMATICA)

$$\int_{-\infty}^{\infty}dq_x\frac{1}{q_x^2}(1-\cos[q_x x])=\pi|x|, \tag{A6}$$

while the second gives

$$\int_{-\infty}^{\infty}dq_x\int_0^Z dZ'\frac{\partial f}{\partial Z'}=\int_0^Z dZ'\int_{-\infty}^{\infty}dq_x e^{-Z'q^2}\cos[q_x x] = \int_0^Z dZ'\sqrt{\pi/Z'}\exp -x^2/(4Z'). \tag{A7}$$

After elementary rearrangements, the remaining integral over Z' can be linked to the definition of the error function $\mathrm{erf}(x)=2/\sqrt{\pi}\int_0^x dt\exp[-t^2]$,

$$\langle \tfrac{1}{2}q_0^2|u(x,z)-u(0,0)|^2\rangle = -\eta\frac{2\pi}{\lambda}\sqrt{\pi\lambda|z|}\ \ e^{-x^2/(4\lambda|z|)} - \eta\frac{\pi^2}{\lambda}|x|\mathrm{erf}\left(\frac{|x|}{2\sqrt{\lambda|z|}}\right), \tag{A8}$$

which in the harmonic approximation of Eq. (17) leads to the correlation function of a 2D smectic as given by Eq. (4) in Sec. III.

APPENDIX B: COMPRESSIBILITY OF A LINEAR ARRAY OF LINE CHARGES

In this appendix we calculate the compressional modulus $B(d)$ for a system of equally spaced line charges of charge density λ(C/m) in between homogeneously charged planes of sheet density σ(C/m^2). This may be a valid approximation for the present case of DNA intercalated in between cationic lipid membranes, if no neutral colipid is present or if the lipids do not demix.

Since the field is constant in between parallel and uniformly charged planes, the only effect of the lipid bilayers in this electrostatic *jellium model* is to fix the average spacing d between the DNA to maintain overall charge neutrality. B is then determined by the restoring force per unit length that arises from a small displacement Δ, e.g., of one strand with respect to the linear array. In this simplified picture the logarithmic potential of all the strands can be summed up to give

$$B=\frac{\pi\lambda^2}{6\epsilon d}, \tag{B1}$$

with λ the line density of charges of the DNA (e/1.7 Å), e the unit charge, and $\epsilon=\epsilon_0\epsilon_r$ the dielectric constant of the water in between the DNA. This model can then be applied to samples of only cationic lipid ($\nu=0$), i.e., the first data point in Fig. 14, yielding $B=2.74\times10^{-2}kT/\text{Å}^2$ for $\lambda=e/1.7$ Å, $d=27$ Å, and $\epsilon_r=80$. The measured value of $B=(3.77\pm0.3)\times10^{-2}kT/\text{Å}^2$ is somewhat larger than this prediction, which can be easily attributed to hydration forces, as discussed in Sec. V. Moreover, the above equation compares well with the experimental $B(d)$ values over the whole range. Without adjustable parameters, the prefactor of the $1/d$ dependence is fairly close to the emperical coefficient C in Fig. 17(b) found by a free fit. Thus, the present ''jellium model'' without any adjustable parameter predicts a result well in agreement with the data. In reality, however, the assumption of a perfectly homogeneous charge density in the

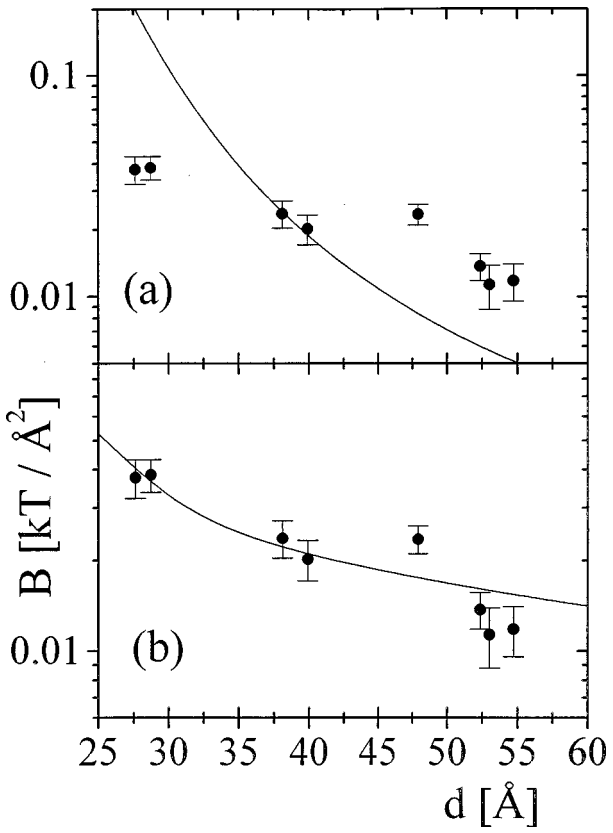

FIG. 17. The experimental data $B(d)$ with a fit to (a) hydration, van der Waals, and electrostatic (Poisson-Boltzmann) forces. The parameters have been varied within physically reasonable values (see text). Clearly, the theory predicts a much stronger decay of $B(d)$ than observed. (b) If instead of the Poisson-Boltzmann result an empirical $1/d$ term is included, reasonable agreement is obtained.

lipid membrane may no longer be valid, if a local compression or decompression of the DNA due to thermal fluctuations is accompanied by a corresponding change of lipid area headgroup to maintain local charge neutrality. More importanly, any lateral demixing of charged and uncharged lipids will contradict the central assumption of charge homogeneity in the membrane. The mixing enthalpy is not likely to be large enough to prevent the lipids from charge seggregation [47]. However, even though applicability of this simple electrostatic model remains doubtful for samples with neutral colipid $\nu \neq 0$, it provides an excellent result when compared to the measured $B(d)$ values.

To derive the above equation, we assume the negative line charges to be placed on a one-dimensional lattice with periodicity d in each of the line charge layers. Since we further assume the line charges to be perfectly uncorrelated across different layers, it is sufficient for the calculation of averaged elastic constants to consider only one layer of line charges with planes of half the charge density $\sigma/2$ on each side. However, the field between equally charged planes is zero, so that we can ignore the presence of the positive sheet charges altogether. Their only effect is to fix the value of d to ensure overall charge neutrality. Thus we are left to evaluate the compressibility of parallel and equally spaced line charges in 2D.

Due to the logarithmic form of the potential of a line charge [44] $V(r) = -\lambda/(2\pi\epsilon)\ln(r)$, with ϵ the dielectric constant of the medium, the total energy of such an array diverges. However, one can calculate the change in energy with respect to the ground state if the position of one line charge is displaced by Δ along z with respect to the perfect lattice site. Labeling the corresponding line with $n=0$, one can sum up the terms corresponding to the difference in potential energy (per unit length along the lines in the x direction) for each of the other line charges on the left- and right-hand side, respectively,

$$\Delta U_n = \frac{\lambda^2}{2\pi\epsilon}(\ln|nd| - \ln|nd-\Delta|), \qquad \Delta U_{-n} = \frac{\lambda^2}{2\pi\epsilon}(\ln|nd| - \ln|nd+\Delta|). \tag{B2}$$

Adding the terms by pairs of $\pm n$, one gets

$$\Delta U = \sum_{n=1}^{\infty} \frac{\lambda^2}{2\pi\epsilon}\left[\ln\left(\frac{|nd|}{|nd-\Delta|}\right) + \ln\left(\frac{|nd|}{|nd+\Delta|}\right)\right] \overset{\Delta \ll d}{=} \sum_{n=1}^{\infty} -\frac{\lambda^2}{2\pi\epsilon}\frac{\Delta^2}{d^2 n^2} = -\frac{\lambda^2}{12\pi\epsilon}\frac{\Delta^2}{d^2}, \tag{B3}$$

where first a Taylor expansion valid for small Δ was used and for the last step the relation $\Sigma_{n=1}^{\infty}(1/n^2) = \pi^2/6$. The result is of the harmonic form $\Delta U \propto \Delta^2$ defining a force constant $k = \lambda^2/6\pi\epsilon d^2$ and the corresponding compressional modulus $B = dk = \lambda^2/(6\pi\epsilon d)$.

[1] J. Rädler, I. Koltover, T. Salditt, and C. R. Safinya, Science **275**, 810 (1997).

[2] T. Salditt, I. Koltover, J. Rädler, and C. Safinya, Phys. Rev. Lett. **79**, 2582 (1997).

[3] P. L. Felgner *et al.*, Proc. Natl. Acad. Sci. USA **84**, 7413 (1987); P. L. Felgner and G. Rhodes, Nature (London) **349**, 351 (1991); A. Singhal and L. Huang, in *Gene Therapeutics: Methods and Applications of Direct Gene Transfer*, edited by J. A. Wolff (Birkhauser, Boston, 1994).

[4] R. Bruinsma and J. Marshl, Europhys. Lett. **41**, 165 (1998); R. Bruinsma (unpublished).

[5] C. S. O'Hern and T. C. Lubensky, Phys. Rev. Lett. **80**, 4345 (1998).

[6] L. Golubović and M. Golubović, Phys. Rev. Lett. **80**, 4341 (1998).

[7] N. Dan, Biophys. J. **73**, 1842 (1997).

[8] E. Sackmann, Science **271**, 43 (1996); H. E. Warriner, S. H. J. Idziak, N. L. Slack, P. Davidson, and C. Safinya, *ibid.* **271**, 969 (1996).
[9] For a recent review see, e.g., R. H. Austin, J. P. Brody, E. C. Cox, T. Dike, and W. Volkmuth, Phys. Today **50**, 32 (1997).
[10] T. T. Perkins, E. S. Douglas, and S. Chu, Science **264**, 819 (1994).
[11] P. J. Hagerman, Annu. Rev. Biophys. Biophys. Chem. **17**, 265 (1988); S. B. Smith, L. Finzi, and C. Bustamante, Science **258**, 1122 (1992).
[12] V. A. Bloomfield, Biopolymers **31**, 1471 (1991).
[13] F. Livolant and M. F. Maestre, Biochemistry **27**, 3056 (1988); R. Podgornik, D. C. Rau, and V. A. Parsegian, Macromolecules **22**, 1780 (1989); Z. Reich, E. J. Wachtel, and A. Minsky, Science **264**, 1460 (1994).
[14] R. D. Kamien and D. R. Nelson, Phys. Rev. E **53**, 650 (1996).
[15] A. Caillé, C.R. Seances Acad. Sci., Ser. A **274**, 891 (1972).
[16] J. Als-Nielsen, J. D. Litster, R. J. Birgenau, M. Kaplan, C. Safinya, A. Lindegaard-Andersen, and S. Mathiesen, Phys. Rev. B **22**, 312 (1980).
[17] C. R. Safinya, E. B. Sirota, D. Roux, and G. S. Smith, Phys. Rev. Lett. **62**, 1134 (1989); **57**, 2718 (1986).
[18] K. Morishige, J. Chem. Phys. **100**, 3252 (1994).
[19] L. Golubović and Z.-G. Wang, Phys. Rev. E **49**, 2567 (1994).
[20] G. S. Manning, J. Chem. Phys. **51**, 924 (1969).
[21] I. Koltover, T. Salditt and C. R. Safinya (unpublished).
[22] M. Dubois and T. Zemb, Langmuir **7**, 1352 (1991).
[23] R. T. Zhang, R. M. Suter, and J. F. Nagle, Phys. Rev. E **50**, 5047 (1994), and references therein.
[24] V. M. Kaganer, B. I. Ostrovskii, and W. H. de Jeu, Phys. Rev. A **44**, 8158 (1991).
[25] N. Lei, C. R. Safinya, and R. F. Bruinsma, J. Phys. II **5**, 1155 (1995).
[26] L. D. Landau and E.M. Lifschitz, *Statistical Physics* (Pergamon, Oxford, 1980).
[27] S. G. J. Mochrie, A. R. Kortan, R. J. Birgeneau, and P. M. Horn, Z. Phys. B **62**, 79 (1985).
[28] MATHEMATICA 2.0, Wolfram Research Inc., 1991.
[29] P. Dutta and S. K. Sinha, Phys. Rev. Lett. **47**, 50 (1981).
[30] I. S. Gradsteyn and I. M. Rhyzhik, *Table of Integrals, Series, and Products* (Academic Press, San Diego, 1979).
[31] O. Stier and V. Türck, OPTIMIZE 4.0, 1996.
[32] G. Grinstein and R. A. Pelcovits, Phys. Rev. Lett. **47**, 856 (1981).
[33] Y. Fang and J. Yang, J. Phys. Chem. (to be published).
[34] S. F. Edwards and D. R. Wilkinson, Proc. R. Soc. London, Ser. A **381**, 17 (1982).
[35] T. Salditt, T. H. Metzger, and J. Peisl, Phys. Rev. Lett. **73**, 2228 (1994); T. Salditt, D. Lott, T. H. Metzger, J. Peisl, G. Vignaud, P. Høghøj, O. Schärpf, P. Hinze, and R. Lauer, Phys. Rev. B **54**, 5860 (1996).
[36] X. Grosberg and X. Khokhlov, *Statistical Physics of Macromolecules* (AIP, New York, 1993).
[37] W. Helfrich, Z. Naturforsch. A **33a**, 305 (1978).
[38] B. Beblick, R. M. Servuss, and W. Helfrich, J. Phys. (France) **46**, 1773 (1985).
[39] D. Sornette and N. Ostrowsky, J. Phys. (France) **45**, 265 (1984).
[40] D. Roux and C. Coulon, J. Phys. (France) **47**, 1257 (1986).
[41] K. Nisizima, Prog. Theor. Phys. **85**, 39 (1991).
[42] R. Podgornik, D. C. Rau, and V. A. Parsegian, Biophys. J. **66**, 962 (1994); D. C. Rau, B. Lee, and V. A. Parsegian, Proc. Natl. Acad. Sci. USA **81**, 2621 (1984).
[43] H. H. Strey, V. A. Parsegian, and R. Podgornik, Phys. Rev. Lett. **78**, 895 (1997), and references therein.
[44] E. Durand, *Electrostatique* (Masson, Paris, 1964), Tome I.
[45] D. Roux and C. R. Safinya, J. Phys. (France) **49**, 307 (1988).
[46] See, for example, J. Israelachvili, *Surface and Intramolecular Forces* (Academic Press, London, 1992).
[47] D. Harries, S. May, W. M. Gelbart, and A. Ben-Shaul, Biophys. J. (to be published).